water

MDPI

Article

Impacts of the Degraded Alpine Swamp Meadow on Tensile Strength of Riverbank: A Case Study of the Upper Yellow River

Haili Zhu [1], Peng Gao [2,*], Zhiwei Li [3], Jiangtao Fu [4], Guorong Li [1], Yabin Liu [1], Xilai Li [5] and Xiasong Hu [1]

1 Department of Geological Engineering, Qinghai University, Xining 810016, China; qdzhuhaili@163.com (H.Z.); qdliguorong@163.com (G.L.); liuyabingqh@sina.com (Y.L.); huxiasong@sina.com (X.H.)
2 Department of Geography, Syracuse University, Syracuse, NY 13244, USA
3 State Key Laboratory of Water Resources and Hydropower Engineering Science, Wuhan University, Wuhan 430072, China; lizw2003@whu.edu.cn
4 School of Civil Engineering and Architecture, Shaanxi University of Technology, Hanzhong 723000, China; fujiangtao865@sina.com
5 College of Agriculture and Animal Husbandry, Qinghai University, Xining 810016, China; Xilai-li@163.com
* Correspondence: pegao@maxwell.syr.edu; Tel.: +1-315-436-5895

Received: 1 July 2020; Accepted: 18 August 2020; Published: 21 August 2020

Abstract: In the meandering riverbank of the Upper Yellow River (UYR), the native alpine swamp meadow (AS) has continuously degenerated into an alpine meadow (AM) due to climate change and intensified grazing. Its implication on river morphology is still not well known. This study examined this effect by in situ measurings of (1) physical properties of roots and their distribution in the soil-root mixture of the upper bank layer, and (2) the tensile strength in terms of excavating tests for triggering cantilever collapses of AS and AM riverbanks. The results showed that the root number in AS was significantly greater than that in AM, though the root distribution in both was similar. Also, the average tensile strength of individual roots in AS was 31,310 kPa, while that in AM was only 16,155 kPa. For the soil-root mixture, it decreased from 67.39 to 21.96 kPa. The weakened mechanical property was mainly ascribed to the lessened root number and the simpler root structure in the soil-root mixture of AM that reduces its ability to resist the external force. These findings confirmed that healthy AS can enhance bank stability and delay the development of tensile cracks in the riverbank of the meandering rivers in the UYR.

Keywords: alpine swamp meadow; alpine meadow; degradation of riparian vegetation; root distribution; tensile strength; tensile crack

1. Introduction

Banks of meandering rivers are often composed of silts and sand that have significantly higher compressive strength than tensile strength or cohesion [1–4]. There has been a consensus that riparian vegetation can reinforce bank strength [5–9] and stability through the interaction between soil and roots [10–16]. Mechanisms of riverbank failure are quite different from those found on hillslopes because steeper and shorter riverbanks tend to have a more variable profile and relatively small size of the failed block [17]. Accordingly, vegetation types and their root distributions throughout the bank profile play a critical role in resisting riverbank failure. In addition, the lower soil layer of the composite riverbank is subject to fluvial erosion, often resulting in a cantilever upper layer that includes the mixture of cohesive soil and vegetation. Once the gravity moment generated by the upper cantilever

layer exceeds its tensile moment, vertical cracks are developed and continuously extend through the upper layer, causing cantilever bank failure [10,18]. The ability of the soil-root mixture to resist external forces is a key factor in evaluating the bank stability.

Many studies have analyzed the tensile strength of fiber-reinforced soils and explored its relationship with soil physical indices using laboratory experiments [19–23]. These studies found that the benefits of natural or synthetic fiber reinforcement include (1) improved ductility in tension compared with pure earth blocks and (2) inhibition of tensile crack propagation [21–24]. Since the root system is intertwined in the soils, artificial soil blocks remolded in these laboratory experiments cannot reflect the actual root branching structure and the complex interaction between roots and soils. It is thus imperative to perform in situ tensile tests using naturally rooted soils for revealing the tensile properties of riparian vegetation.

In recent decades, a series of studies have been carried out for examining the shear strength of rooted soils using either in situ or indoor shear-test experiments. These studies helped better understand the enhancement of the vertically extending root system through soils by revealing that coarse roots tend to stabilize the soil-root mixture and fine roots may enhance its mechanical strength [25–27]. Other studies have confirmed that the number of roots passing through the potential shear plane, root system distribution and its strength [27,28], the initial water content of the soils [12,29], and the soil-root friction [30], contribute to soil reinforcement. However, there is still a lack of studies for quantifying the tensile strength of the rooted soil and the reinforced traction in the soil-root mixture.

The Upper Yellow River (UYR) watershed is located in the hinterland of the Qinghai-Tibet Plateau and includes numerous rivers, lakes, and wetlands. It is an important source of fresh water but a fragile ecosystem in the western region of China. When the UYR flows from the source into the open terrain with low-lying hills and valleys on the eastern edge of the Qinghai-Tibet Plateau, it forms a unique curved shape in plane form, commonly called the first bend of the UYR [31]. Meandering rivers are widely developed in this area, accompanied by the vegetation cover of the alpine swamp meadow and its degraded type, the alpine meadow. Because of global climate change and anthropogenic disturbances, the alpine swamp meadow on the eastern Qinghai-Tibet Plateau has been undergoing severe degradation [32–35]. The degradation succession of the alpine swamp meadow caused changes in the composition of the plant community. Dicotyledonous plants with a straight root system replaced sedges and gramineous plants with a dense clump root system, leading to changes in the underground biomass of the plant community, reduction of the spatial distribution of the root system, and a significant decrease of root activity and bulk density [35,36]. The biological degradation affects not only the root distribution of riparian vegetation but also the tensile and shear strength of the vegetated riverbanks. This means that degraded riparian vegetation could decrease bank stability and affect lateral evolution trends of meandering rivers in the UYR. Therefore, quantifying the influence of alpine swamp meadow degradation on the strength of riverbank soils in the UYR is an important issue that needs to be addressed. Most previous studies have examined the shear strength of the vegetated soils [8–13,16,25,26,37]. Little has been done on quantifying the effect of degraded riparian vegetation on the tensile strength of the soil-vegetation mixture.

In this study, we addressed this issue by focusing on the riverbanks of a meandering reach that has initially formed a cantilever arm under fluvial erosion. The vegetation community is featured by a healthy alpine swamp meadow (AS) and moderately degraded alpine meadow (AM). We measured root numbers and their vertical distributions in the soil-root mixture within a depth range of 0.3 m. Furthermore, by excavating the sandy layer below the top soil-vegetation layer of the bank in situ for artificially initiating cantilever bank collapse, we measured the tensile strength of individual roots using in situ pullout tests and subsequently calculated that for the soil-root mixture of the collapsed bank blocks. By comparing the differences of these results between AS and AM mixtures, we revealed the effects of meadow degradation on bank tensile strength and the role of roots in slowing bank crack development.

2. Experiences at Field Scale and Procedure for Determining the Cantilanver Bank Collapse

2.1. Study Sites and Degradation of Alpine Swamp Meadow

The Upper Yellow River (UYR) watershed is within the Qinghai-Tibet Plateau located in western China (Figure 1a). In its downstream reach, the main channel is joined by a relatively small tributary, the Lanmucuo River (Figure 1b). Our study sites are in the upstream reach of this tributary (34°26′ N–35°02′ N; 101°29′ E–101°35′ E) (Figure 1c). This reach has elevations ranging between 3400 and 4200 m a.s.l. with a mean channel gradient of 0.19%. The UYR region is subject to the alpine monsoon climate that features a long, cold dry season from October to early May, and a short, warm wet season from middle May to September. The annual mean precipitation is 560.5 mm [38], most of which is concentrated in the period from June to September, accounting for more than 83% of the total. The annual mean evaporation and temperature are 1278 mm and −0.16 °C, respectively [39]. Under this climate, the ground consists of seasonally frozen soils.

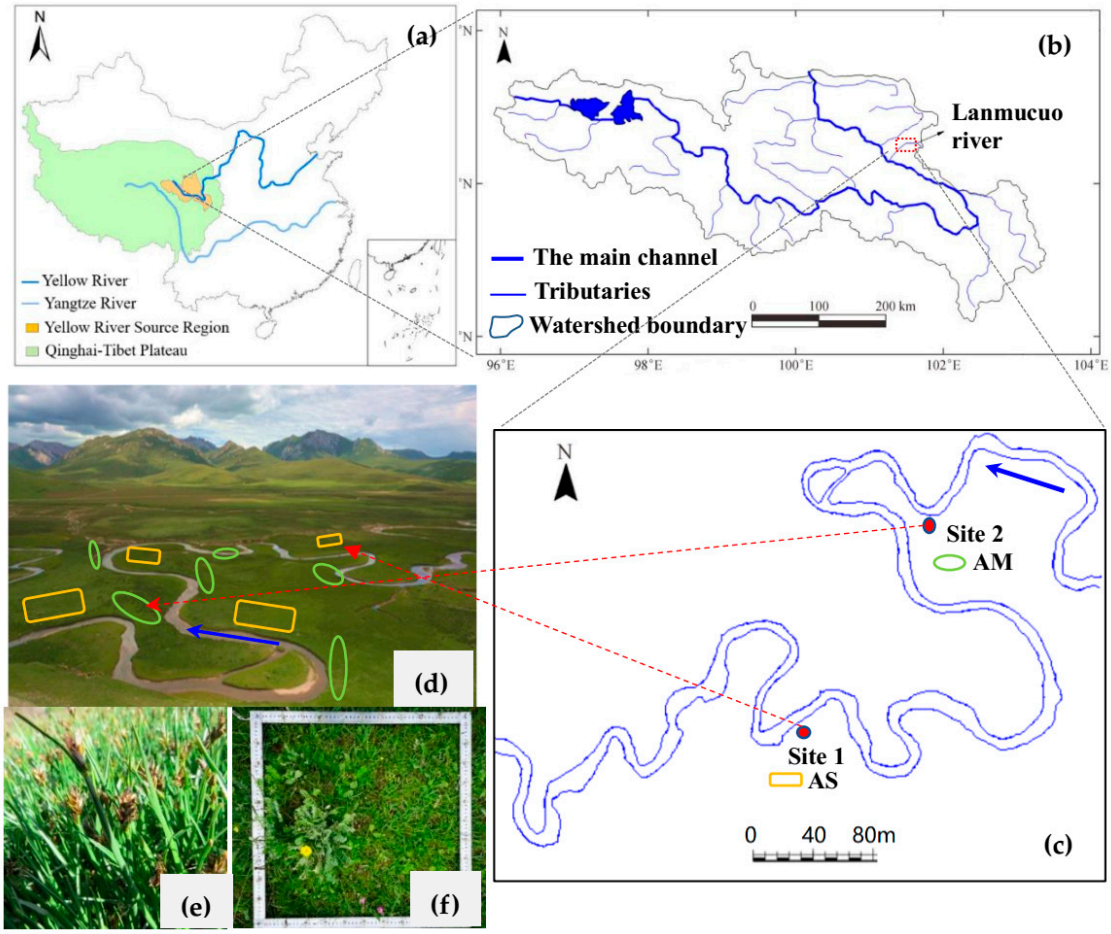

Figure 1. (**a**) The geography of the Qinghai-Tibet Plateau and Upper Yellow River; (**b**) the location of the study area in the Lanmucuo river; (**c**) the specific locations of the two selected sites; (**d**) the spatially distributed AS and AM along the riparian zone of the Lanmucuo River; (**e**) illustration of *Blysmus sinocompressus*, the dominant species of AS; (**f**) demonstration of the AM that is rich in species composition (some degraded species are discernable).

Grassland is the major type of land cover in the region. It is dominated by alpine swamp meadow (AS), which provides important ecosystem services to the regional environment. Affected by global warming and intensified grazing, AS in the region has gradually degraded to alpine meadows (AM) and alpine steppe meadows (ASM) [40]. Spatially, AS and AM are often seen along riverbanks,

the Lanmucuo River, while ASM is mostly distributed on the upper sloping parts of the piedmonts (Figure 1d). Because the area covered by ASM is far away from river banks, it is not a concern in this study. Based on a set of qualitative and semi-qualitative indicators used for pasture degradation classification [33,35], a survey for riparian vegetation along a 22 km reach of the upper Lanmucuo River was conducted in the 2017–2019 period [16,41]. During the survey, the coverage and number of species, dominant species, and underground biomass of AS and AM were determined within each sampling plot with the size of 1 × 1 m. The underground biomass was represented by the root mass within the soil layer that is 0.3 m in depth. The results (Table 1) showed that the values of all measured metrics were different with statistical significance between AS and AM.

Table 1. Characteristics of the surveyed AS and AM communities in the study area.

Vegetation Type	Coverage (Mean ± SD *, %)	Number of Species (Mean ± SD)	Under-Ground Biomass (g m^{-2})	Dominant Species	Number of Surveyed Sites
AS	96.3 ± 2.7 ^{a}	3.5 ± 2.7 ^{b}	378 ± 74 ^{a}	*Blysmus sinocompressus*	40
AM	74.5 ± 11.6 ^{b}	14.8 ± 5.1 ^{a}	193 ± 56 ^{b}	*Kobresia pygmaea* *Elymus nutans* *Potentilla saundersiana*	44

* standard deviation; AS: alpine swamp meadow; AM: alpine meadow; Different superscripts of a and b denote significant differences ($p < 0.05$) between different vegetation types.

In general, distributions of surficial plant species, coverage, and rooting depth and lateral root spread in underground root systems are determined by the prevailing physical habitats [42]. In particular, AS tends to appear in areas with topographic lows and occupied by seasonally saturated water (i.e., in swales), whereas AM is typically developed around the apex of river bends (Figure 1d). Vegetation communities of AS are mainly composed of cold-tolerant hygrophytes and hydromesophytes, which have a simple community structure. *Blysmus sinocompressus* is the dominant and healthy specie (Figure 1e and Table 1) and its coverage reaches nearly 98%. The remaining 2% is contributed from other species, such as *Ranunculus nephelogenes* and *Pedicularis longiflora*. The dominant species of AM are *Kobresia pygmaea*, *Elymus nutans*, and *Potentilla saundersiana*, accounting for 30% of the coverage (Table 1). Other herbaceous species, such as *Poa annua*, *Nardostachys jatamansi*, *Saxifraga montana*, *Aconitum tanguticum*, and degraded species, such as *Leontopodium pusillum*, *Oxytropis ochrocephala*, take up to 30% of the coverage. This means that AM only takes 60% of the habitat (Figure 1f). Compared with AS, the number of species and the mesophytes in AM are significantly high (Table 1). These surficial ecological differences between AS and AM must affect their underground properties and the associated mechanical characteristics, which were investigated in this study.

2.2. Field Experiments and Measurements

Field experiments were conducted at the two selected sites that are about 200 m apart from each other in the study area (Figure 1c). These sites have natural vegetation communities and are not disturbed by livestock and human activities. Therefore, they are representative of the general vegetation distribution in the study area. Site 1 is covered by AS, while site 2 is topped by AM. The height of the riverbank to the water level of the channel flow at site 1 is about 0.2–0.4 m lower than that at site 2, suggesting that the groundwater level at site 1 is higher than that at site 2. This ·difference is the main factor that determines the spatial distribution of AS and AM in the study area. The riverbank at both sites had been undercut by river flows, forming a cantilever arm with a width of about 0.2 m and thickness of about 0.3 m at site 1, while 0.3 and 0.35 m, respectively at site 2 (Figure 2). Both cantilever arms were stable with no tensile cracks developed on the top. They were underlined by a layer of silt and sand with a thickness of approximately 0.3 to 0.6 m, whose bottoms were gradually intergraded into fine gravels deposited at the toes of both banks (Figure 2). Field experiments were conducted during an October storm event in 2018, such that the entire bank profiles were exposed, facilitating subsequent bank excavation and measurements.

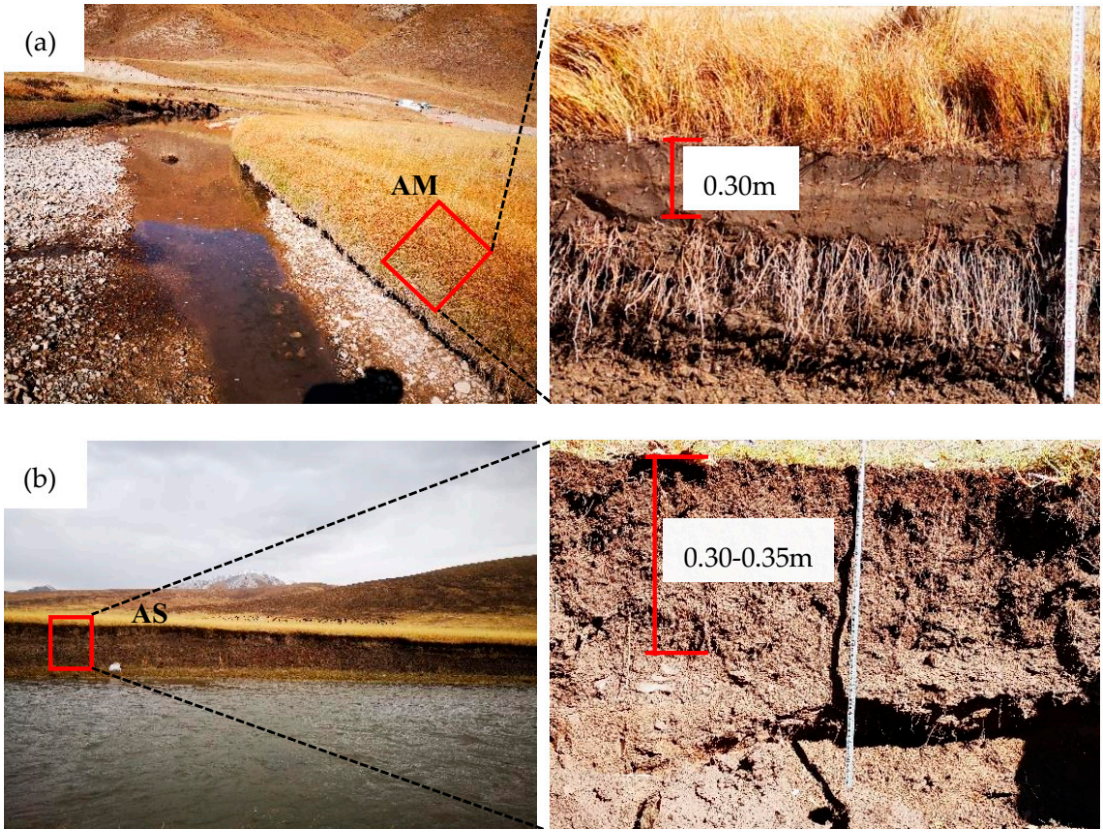

Figure 2. Riverbanks and their vertical profiles at (**a**) site 1, which is covered by AS, and (**b**) site 2, which is covered by AM (not to scale).

At each site, experiments were performed at the face of a bank profile stretched longitudinally for 8 m (Figure 3). An area of 1 m long on each side (i.e., E1 and E2 in Figure 3) was selected for extending the existing cantilever arm by excavating the lower part of the bank profile. The two areas were selected apart from each other by 3 m to ensure that the excavation of the first one would not affect the stability of the second. During each experiment, excavation was executed gradually, such that the development of tensile cracks on top of the cantilever arm could be observed. Their emergence indicated the status of arm stability. Excavation ended when the cantilever arm reached the threshold that triggered the failure of the cantilever arm. Three types of measurements were subsequently performed after bank collapse, determining tensile strengths of individual roots, measuring root diameter, number, and distribution, and sampling soil for both in situ and laboratory analyses.

The tensile strength of a single root for a given plant species (T_r, MPa) may be determined by [2],

$$T_r = 4F/(\pi d^2) \quad (1)$$

where F is the maximum pullout force of measured individual roots (N) and d is the diameter of the corresponding single root (10^{-3} m). The value of F was measured using a HP-500 digital push-pull meter with a maximum load of 500 N and an indication error of ±0.5% (Leqing Aidebao Instruments Co. Ltd., Leqing, China). This measurement was taken at three plots within the experimental area; two (i.e., R1 and R3) were on the new face of the upper soil-root layer after cantilever failure and the other (i.e., R2) was at the face of the original upper bank (Figure 3). This design assured that the measured tensile strength accounted for spatial variability. At each plot, vegetation roots were separated from their surrounding soils by brushing soil particles away. Then, every single root was connected to the tension meter by a clamp. The value of F was recorded after applying a horizontal tensile force at a uniform speed until the root is broken or pulled out (Figure 4). The diameter of the

same root was also measured using a Vernier caliper with an accuracy of 2×10^{-5} m. If the broken position of the root was close to the clamp, then the recorded F value was biased and not counted. There were more than 30 roots measured in each plot.

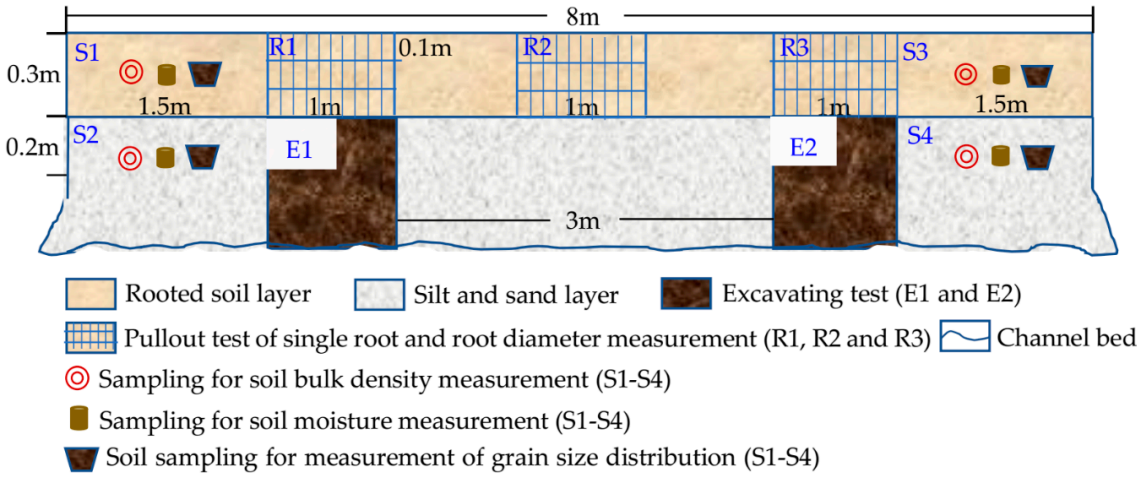

Figure 3. The design of bank excavation experiments and other measurements.

Figure 4. Measuring the maximum pullout force of individual roots using a tension meter.

Root diameters and numbers were measured within the front faces of the soil-root layer (0.3 m in thickness) in the collapsed bank block at R1 and R3, and the face of the same layer in the original bank at R2 (Figure 3). The surface of the face was washed by water to expose the root system and then divided into 30 small zones by laying a grid whose cells had the size of 0.10 × 0.10 m on the top. Within each of the 30 cells, root diameters were measured using the same Vernier caliper and the number of roots was recorded. All the roots that passed through the soil-root layer were measured. These values were classified into three groups based on the root diameter (i.e., <0.5, 0.5–1.0, and >1.0 × 10^{-3} m), and the depths with the soil-root layer (i.e., 0–0.10, 0.11–0.20, and 0.21–0.30 m). The root area ratio (RAR), defined as the ratio of the total area of all roots passing through the collapsed soil-root layer to the area of the plot (i.e., 1 × 0.3 m), was then calculated using the measured values. The measurements were repeated three times at each plot (i.e., R1, R2, and R3).

Soil samples were taken from two small plots in the soil-root layer around the depth of 0.10–0.20 m beneath the ground surface (i.e., S1 and S3 in Figure 3) and from two plots in the lower layer between 0.3 and 0.5 m from the ground surface (i.e., S2 and S4 in Figure 3) at both sites. These samples were carefully stored and transported back to the soil mechanics laboratory of Geological Engineering Department, Qinghai University for further analysis. The oven-drying method [43] was used to determine the soil moisture content, and the sieving method [43] was applied to determine the grain size distribution. Each measurement was repeated three times for accuracy. Additionally, a cutting

ring with a capacity volume of 6.0×10^{-5} m^3 was used in situ to determine the soil bulk density at each plot (Figure 3).

2.3. Calculation

In the process of cantilever bank collapse, the weight of the cantilever body is originally balanced by the tensile strength from the soil-root mixture of the body. Extension of the cantilever arm (by artificial excavation in this case or by fluvial erosion under the natural condition) will increase its weight. Once the tensile strength is insufficient to balance the weight, tensile cracks develop from the top of the cantilever body. At this time, both tensile stress and compressive stress exhibit a triangle distribution, and the center axis of the failing cantilever block is located in the stress center of the cantilever body below the crack [44] (Figure 5). Further extension of the cantilever arm catalyzes the development of the tensile crack until the failure of the cantilever body occurs. Under the critical condition of the failure, the external moment of the cantilever body is balanced by the resistance moment of the soil-root mixture, which may lead to [44],

$$Wb_c/2 = \frac{l(d_1 - d_t)^2}{3(1+a)^2}\sigma_t + \frac{a^2 l(d_1 - d_t)^2}{3(1+a)^2}\sigma_c \quad (2)$$

where $W = \rho g b_c d_1 l$ (N) is the weight of the cantilever body; ρ is the bulk density of the soil-root mixture (kg m^{-3}); b_c is the critical width of the cantilever arm (m); d_1 is the thickness of the cantilever layer (m), d_t is the depth of the crack from the top of the bank (m); l is the unit length of the cantilever layer (m), that is 1 m; $a = \sigma_t / \sigma_c$, σ_t and σ_c are tensile and compressive stress of the soil-root mixture (N m^{-2}), following Ajaz's results [45], a = 0.1. Substituting $W = \rho g b_c d_1 l$ into Equation (2), the tensile strength σ_t of the soil-root mixture of the cantilever body may be expressed as

$$\sigma_t = 3(1+a)\rho g {b_c}^2 d_1 / 2(d_1 - d_t)^2 \quad (3)$$

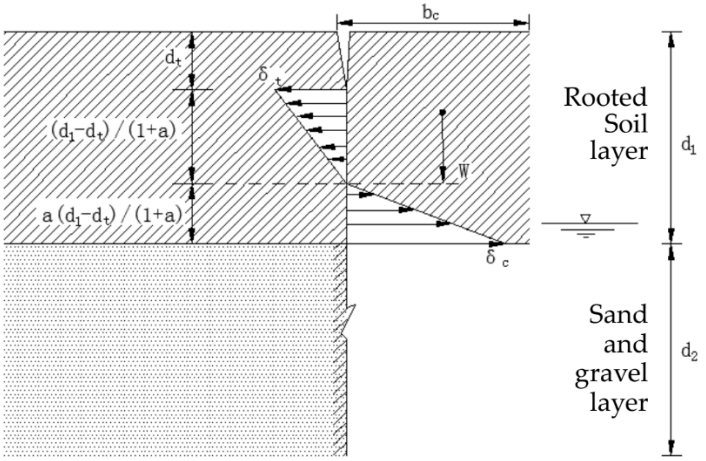

Figure 5. Stress analysis of the upper root-soil layer of a cantilever riverbank (modified from Figure 7 in Xia et al. [44], (not to scale)).

Using the measured d_1 and d_t in our tested AS and AM bank blocks, we calculated their σ_t values. The product of T_r and RAR also reflects the tensile strength of a soil-root mixture. We compared these two types of calculations for the tensile strength.

3. Results and Analysis

3.1. Characteristics of Soils and Root Distribution

Our results demonstrated that the composition and physical properties of the two layers in the vertical profile of the riverbank are significantly different between the two sites (Table 2). Generally, the upper soil-root layer was composed of silt, while the lower layer consisted of silty sand with some poorly graded fine gravel. In the upper layer, the average bulk density and moisture content at the two sites were 1260 kg·m^{-3} and 1560 kg·m^{-3}; 39.36% and 41.72%, respectively. They were about 180 kg·m^{-3} and 405 kg·m^{-3}; 17.12% and 31.42% higher than those in the lower layer. These two soil properties in the soil-root layer of AS were 21.96% and 3.57% higher than those in that of AM. For the lower layer, the average bulk density and moisture content at site 1 were greater than those at site 2 by 118.67% and 3.27%, respectively. It is obvious that the physical parameters (i.e., bulk density and moisture content) of the soil-root mixture of AS and AM are disparate. These differences could have different influences on the tensile strength of the root system in the soil [27], which lend the support for our analyses of tensile strength for both single roots and the soil-root mixture in this study.

Table 2. The physical properties of the two vertical layers at both sites.

Tested Site	Sampling Depth (m)	Soil Type	Bulk Density ρ (kg·m^{-3})	Moisture Content ω (%)	RAR (%)
1(AS)	0.10–0.20	Silt	1560	41.71	0.22
	0.30–0.40	Silty sand	1730	10.29	-
2(AM)	0.10–0.20	Silt	1550	40.92	0.23
	0.30–0.40	Silty sand	1740	10.97	-
	0.10–0.20	Silt	1260	40.42	0.12
	0.40–0.50	Silty sand	1710	24.25	-
	0.10–0.20	Silt	1290	39.36	0.11
	0.40–0.50	Silty sand	1650	22.24	-

Although the distribution of roots over different classes of root diameters is highly variable for different species [46], it may still be characterized by vertical patterns of root number and diameters along the depth of a riverbank. In this study, AS is mainly composed of *Blysmus sinocompressus*, belonging to the *Cyperaceous* family. This species has a typical dense and fibrous root system that may be up to 0.8 m long, and its rhizomes are typically about 0.25–0.60 m long. These roots mix with the surrounding soil, forming a soil-root layer that extends from the bank surface to the depth of 0.30 m. Our results showed that the total root number within the experimental block of this layer, which was 1.0 m long and 0.3 m deep (Figure 3), was 4345, with 2505, 1160, and 680 in the depth ranges of 0–0.10, 0.11–0.20, and 0.21–0.30 m, respectively. Among these roots, those with the root diameter <0.5, 0.5–1.0, and >1.0 × 10^{-3} m took about 66%, 25%, and 9%, respectively. AS is dominated by finer roots, which is evidenced by the fact that within each of the three depth ranges, they took 66%, 67%, and 76%, respectively (Figure 6a). Roots with medium diameters (0.5–1.0 × 10^{-3} m) in all three depth ranges took about 25%, while those with the diameters >1.0 × 10^{-3} m only existed in the depths of 0–0.10 and 0.11–0.20 m, taking merely 9% and 8%, respectively. More fine roots (<0.5 × 10^{-3} m) developed in the shallow depth range rather than in the deep depth range, supported by their distributions of 56%, 26%, and 18% in the depth ranges of 0–0.10, 0.11–0.20, and 0.21–0.30 m, respectively (Figure 6a). The roots with the mean diameter (0.5–1.0 × 10^{-3} m) followed a similar vertical distribution, featured by 58%, 27%, and 15% in the three depth ranges, respectively. Roots with the diameters >1.0 × 10^{-3} m only existed in the first two depth ranges with 71% and 29%, respectively.

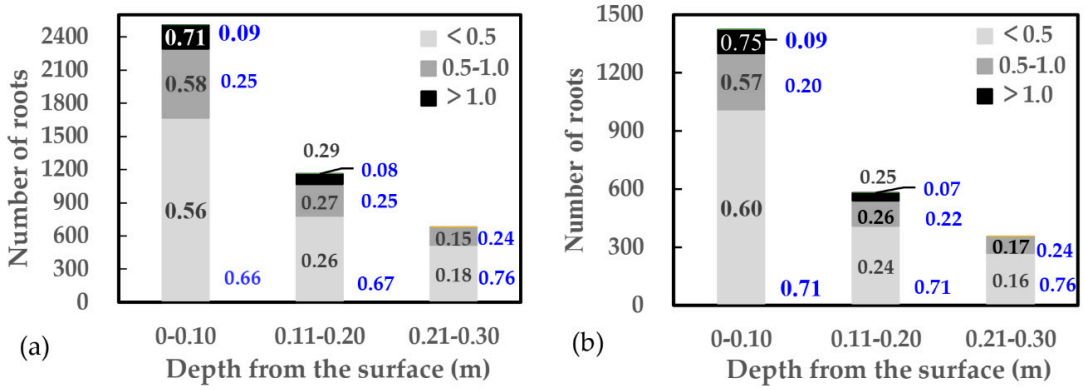

Figure 6. Root distributions in the three depth ranges of the experimental blocks for (**a**) AS and (**b**) AM. The number within each color of the three columns represents the percentage of roots in each sub-layer of the soil-root layer (i.e., the sum of the numbers in each color is 100%). The number outside of the columns represents the percentages of three root diameters in each sub-layer (i.e., the sum of these numbers along each column is 100%). The scaling of the y-axis is different between (**a**,**b**).

The AM is dominated by *Kobresia pygmaea, Elymus nutans,* and *Potentilla saundersiana*. Their root number took about 93% of the total in AM. The first two plants have dense and fibrous roots that are about 0.15–0.55 m long. Besides the three dominant plants, AM contains degraded species such as *Nardostachys chinensis*, *Oxytropis ochrocephala*, *Saxifraga montana*, and *Leontopodium pusillum*, whose roots are generally sparse and short. They have a typical tap root system with the length ranging between 0.04 and 0.13 m. The total number of roots in AS was only 2355 with 1420, 580, and 355 in the three depth ranges downward, respectively. Similarly to those in the AS, roots with the diameters $<0.5 \times 10^{-3}$ m dominated in each of the three depth ranges, taking 71%, 71%, and 76%, respectively (Figure 6b). The remaining roots at each depth were those with the mean diameters ($0.5–1.0 \times 10^{-3}$ m). They took roughly the same percentage of the total roots within each depth range, which was 20%, 22%, and 24%, respectively. Again, the coarse roots (i.e., diameter $>1.0 \times 10^{-3}$ m) only occupied the first two depth ranges, taking a small portion of the total roots in each (i.e., 9% and 7%, respectively). Along the vertical direction, roots with each diameter class demonstrated a similar distribution to their AS peers. For example, the fine roots (diameter $<0.5 \times 10^{-3}$ m) took 60%, 24%, and 16% from the top to the bottom depth ranges (Figure 6b). A similar vertical distribution appeared for the roots with the mean diameter (i.e., diameters were between 0.1 and 1.0×10^{-3} m) with 57%, 26%, and 17% in the three depth ranges, respectively. Also, the coarse roots only stayed in the first two depth ranges. Most of them (75%) occupy in the 0–0.10 m depth range (Figure 6b).

Although roots in AS and AM showed similar spatial and diameter distributions, which led to their similar average root diameters (i.e., $0.46 \pm 0.31 \times 10^{-3}$ m and $0.41 \pm 0.39 \times 10^{-3}$ m, respectively) in the entire mixed layer of 0.30 m, their root numbers were greatly different, which can be proved by a two-sample difference test ($p < 0.05$). The root number of AS was 46% higher than that of AM. Consequently, the RAR of the AS experimental block was 0.225% on average, which was about twice that of the AM block (Table 2). These results showed that the root number, which plays an important role in resisting tensile force imposed to the experimental block, is reduced greatly when AS is degraded to AM.

3.2. Tensile Trength of Individual Roots and Soil-Root Mixture

The effect of roots on soil strength of the riverbank does not only depend on the root number, but also the tensile strength of a single root (T_r) (i.e., Equation (1)). The average T_r of the dominant plant *Blysmus sinocompressus*, whose root diameters ranged between 0.20 and 1.76×10^{-3} m at site 1, was 31,310 kPa, and the maximum value can reach up to 128,000 kPa. The T_r for roots with the diameters ranging between 0.24 and 1.88×10^{-3} m at site 2 (i.e., AM) was 16,160 kPa. The average

T_r of the AS block was 48.4% higher than that of the AM block. There existed a strong relationship between the root diameter and T_r (Figure 7), which indicated that T_r decreases as the root diameter increases for both AS and AM. This finding is consistent with those reported in earlier studies [11,46–49]. This relationship may be described by a power function, whose exponent was different between the two sites (Figure 7). For the AS block, when the root diameter was less than 0.70×10^{-3} m, T_r decreased sharply as the root diameter increased, nearly following a linear relationship. Specifically, the value of T_r decreased drastically from 127,930 to 30,810 kPa, as the root diameter only increased from 0.20 to 0.70×10^{-3} m. As the root diameter continuously increased from 0.71 to 1.76×10^{-3} m, T_r only decreased from 26,480 to 7050 kPa. The differences of T_r were 97,120 kPa and 19,430 kPa before and after the threshold root diameter (i.e., 0.7×10^{-3} m). For the AM block, when the diameter was less than 0.4×10^{-3} m, T_r decreased greatly as the root diameter increased, and its value decreased from 73,380 to 23,590 kPa with the average of 39,050 kPa. However, the difference of T_r was only 25,860 kPa when the root diameter increased from 0.4 to 1.88×10^{-3} m. This change was much less than that for root diameters less than 0.4×10^{-3} m (i.e., 49,790 kPa). Therefore, the root diameter of 0.7 and 0.4×10^{-3} m can be taken as a threshold of the AS and AM blocks, respectively. Values of T_r were more sensitive to the changes of root diameters less than the threshold while remaining less variable for coarse roots whose diameters are greater than the threshold.

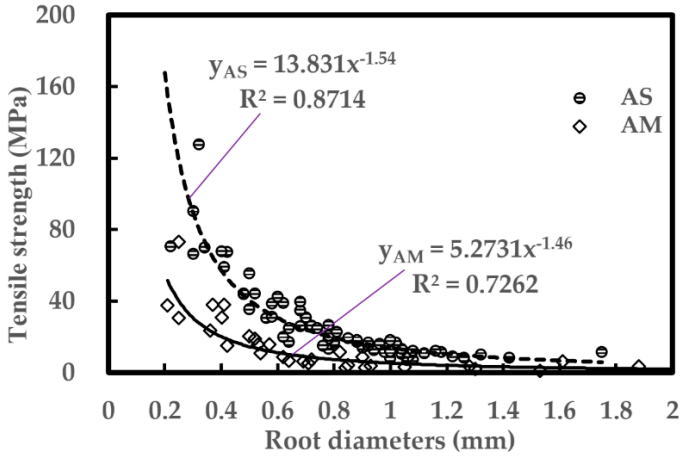

Figure 7. Root tensile strength vs. root diameters for the alpine swamp meadow (AS) and alpine meadow (AM).

Because there were about 93% and 90% fine roots with diameters less than 1×10^{-3} m in the mixed layer of AS and AM blocks, respectively, the difference in the root number should not be the main cause for the different T_r values between AS and AM blocks. Rather, their difference represented the true mechanical discrepancy between the two. In other words, the tensile strength of individual roots in healthy meadow plants (i.e., AS) is generally higher than that in the degraded meadow plants (i.e., AM).

The tensile strength of the soil-root mixture should be relevant to the physical properties of the mixture. At site 1, the moisture content and volume of the two tested bank blocks were different. They were 40.92% and 0.175 m^3 for block 1, and 41.71% and 0.187 m^3 fo block 2, respectively (Tables 2 and 3). The tensile strength of the soil-root mixture (σ_t) between the two tested sites was also slightly different. It was 66.86 kPa for Site 1 and 67.93 kPa for Site 2 (Table 3). At site 2, the moisture content and volume of the two tested experimental blocks were different by 1.06% and 0.004 m^3 (Tables 2 and 3), respectively. However, the variation of σ_t between the two was still minor, merely 1.34 kPa (Table 3). This shows that for either AS or AM, repetitive measurements of σ_t for different experimental blocks were consistent with each other, though the moisture content and volume of the experimental blocks might be slightly different.

Table 3. Physical and mechanical properties of the soil-root mixture at the two sites.

Tested Site	Tensile Strength of Root T_r (kPa)	Thickness of Slump Block d_1 (m)	Crack Depth d_t (m)	Width of Slump Block b_c (m)	Volume of Slump Block V (m^3)	Tensile Strength Based on Formula (3) σ_t (kPa)
1	31,670	0.25	0.035	0.70	0.175	66.86
	30,950	0.26	0.037	0.72	0.187	67.93
mean	31,310	0.255	0.036	0.71	0.181	67.395
2	15,420	0.35	0.048	0.52	0.182	21.29
	16,890	0.35	0.050	0.53	0.186	22.63
mean	16,155	0.35	0.049	0.525	0.184	21.96

These results suggest that variation of the moisture content and volume of the experimental blocks for the same type of plants has a negligible impact on σ_t. Nonetheless, between the AS and AM, the mean tensile strength of the rooted soil was significantly different, which was 67.39 and 21.96 kPa, respectively (Table 3). The value of σ_t for the AS at site 1 was about 3.07 times higher than that of the AM at site 2 (Table 3). The dramatic difference clearly reflected the differences in the mechanical characteristics of the root systems between the AS and AM blocks. It follows that the characteristics of root distribution and tensile strength of individual roots are the important factors that influence the tensile strength of the soil-root mixture.

The product of RAR and T_r is often used to evaluate the contribution of the root system to the soil tensile strength [9,27,49–54]. For a soil-vegetation mixture, the tensile strength is often viewed as that from the soil and root system, and the latter is much greater than the former [9,51]. In this study, the product of RAR and T_r for the AS and AM was 70.45 and 18.58 kPa, respectively. Their ratio was 3.79, which was greater than that of σ_t for the AS and AM blocks (i.e., 3.07) (Table 3). This indicates that conditions of the root system in a soil-root mixture are critical for determining the mechanical characteristic of the mixture.

In the two excavation tests for AS, the depths of the developed cracks in the collapsed block were 0.035 and 0.037 m, respectively, with the average of 0.036 m (Table 3). However, for AM, these depths were 0.048 and 0.050 m, respectively, giving rise to the average of 0.049 m (Table 3). The crack developed in the AM collapsed block was deeper by about 27% than that in the AS block.

4. Discussion

4.1. Effect of Degraded Riparian Vegetation on Tensile Strength of Individual Roots and the Soil-Root Mixture

Continuous vegetation degradation has forced alpine meadow, dominated by members of the Cyperaceae, to transform into bare land and subsequently Heitutan on the Qinghai-Tibet Plateau in western China. Areas of severely degraded alpine meadow on the Qinghai-Tibet Plateau are referred to as Heitutan and are characterized by increased proportions of bare land, reduced edible herbage, and commensurate increases in the dominance of less palatable species [55]. Specifically, when AS degenerates into AM, the distribution of dominant plants reduced significantly, from an original coverage of 98% to only about 30%. This change of the surface vegetation communities has further led to changes in the plant's underground biomass. Our results showed that the root number of AM block was 46% less than that of the AS block within the depth of 0–0.30 m (Figure 6). For plants of AS, many roots were much longer than this depth, some of which may have a length of up to 0.80 m (Figure 2a). For the plants of AM, however, the lengths of most of their roots are less than 0.30 m (Figure 2b). Thus, transforming from AS to AM means that deep-rooted plants with dense root systems are gradually replaced by plants with short and sparse root systems [35,55–58]. This change indicates that the shallow-rooted plants of AM are more vulnerable to high evaporation, livestock trampling, and human activities in the study area, resulting in further degradation [35].

In addition to their different densities and lengths, the two types of plants also have different root structures. The dominant plant of AS (i.e., *Blysmus sinocompressus*) has developed rhizomes. Roots derived from them often grow laterally (Figure 8a). Moreover, some roots have a wave shape (Figure 8a). In AM, however, most roots of the dominant plant (i.e., *Kobresia pygmaea*) grow

vertically with no rhizome (Figure 8b). The other two dominant plants (i.e., *Elymus nutans* and *Potentilla saundersiana*) share a similar root structure. Compared with that of plant roots in AM, the structure of the dominant plant in AS effectively enhances the tensile strength of the soil-root mixture because (1) the laterally distributed roots may increase root density and (2) the wave-shaped roots have greater contact area with the surrounding soils and may resist higher external force by straightening its shape [59].

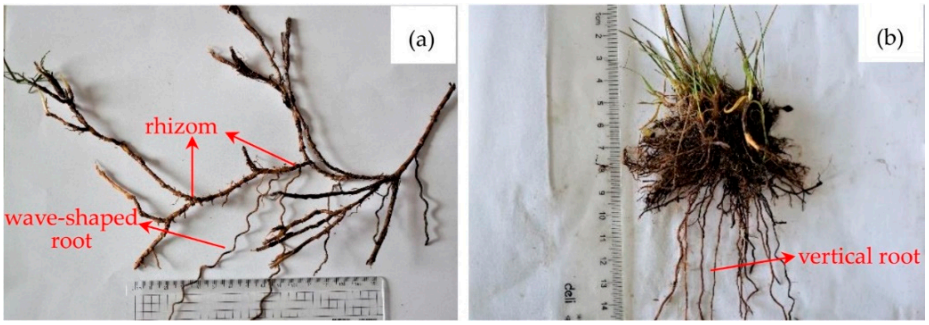

Figure 8. (**a**) The laterally distributed and wave-shaped root system of *Blysmus sinocompressus* in AS; (**b**) the distribution of straight roots in *Kobresia pygmaea* of AM.

The above-mentioned characteristics of root diameters and branching, and the tortuosity of plant roots, mainly affected the mechanical behavior of individual roots [28]. Our study showed that the influence of vegetation degradation is on not only the root number and structure but also on the mechanical characteristics of roots. In the study area, effective roots (i.e., roots with diameters less than 1×10^{-3} m) account for about 93% in the layer of 0–0.30 m (Figure 6) below the surface, indicating that most root systems mainly play the role of reinforcement [60]. When the cantilever arm of the meandering riverbank is formed, the soil and root system is subjected to the external load from the weight of the arm, giving rise to the deformation of the arm. The root system can convert part of the external load into the tensile stress and dissipate it to the surrounding soil through the soil-root interface. In this way, the root system and the surrounding soil particles can work together to balance the load and enhance the soil-root tensile resistance [61].

The tensile strength of the root system is a critical factor that directly reflects the effect of rooted soil consolidation. In our study, the average tensile strength of the root for the dominant plants in the AS reached 31,310 kPa, which was 48% higher than that of the AM (16,155 kPa). Mattia et al. [47] and Li et al. [62] measured the root tensile strength of Gramineae plants of *Lygeum spartum*, *Stipa purpurea* and sedge plant of *Kobresia pygmaea*. They found that their tensile strength ranged from 36,260 to 45,670 kPa, close to that of the sedge plant, *Blysmus sinocompressus* (i.e., 31,310 kPa) in our study. The tensile strength of the root for degraded plants of *Potentilla bifurca*, *Ajania tenuifolia* and *Saussurea salsa* decreases significantly, from 5110 to 25,610 kPa [62]. In our study, this value for the degraded meadow plants (i.e., the AM) was within this range. Evidently, the mechanical characteristics of roots changed because of degeneration. The root tensile strength of healthy meadow plants (i.e., the AS) is much higher than that of the degraded plants (i.e., the AM).

The contribution of the root system to the tensile strength of the rooted soil may be appropriately evaluated using the product of RAR and T_r [9,27,49,51,52]. To further analyze the reduction of the tensile strength in the soil-root mixture due to degradation, we compared our calculated values with those from earlier studies [12,47,62]. All of the products of RAR and root tensile strength of the four degraded herbaceous plants (i.e., 1, 2, 3, 5 in Figure 9) and the AM (i.e., 4) fell in the range of 2.04–38.4 kPa, which are lower than those of four healthy herbaceous plants (i.e., 7, 8, 9, 10 in Figure 9) and the AS (i.e., 6), which are within the range of 72.01–118.74 kPa. Clearly, there is a discrepancy of this product between healthy and degenerated plants, separated by the threshold of 50 kPa (Figure 9).

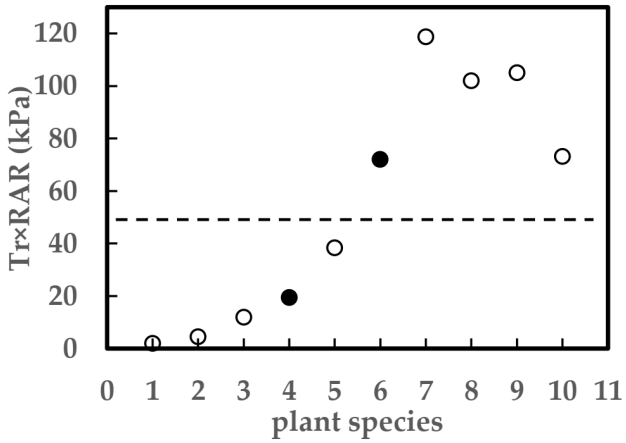

Figure 9. The product of T_r and RAR for healthy and degraded grassland plants. 1. *Saussurea salsa* [62]; 2. *Ajania tenuifolia* [62]; 3. *Potentilla bifurca* [62]; 4. *AM*; 5. *eontopodium nanum* [62]; 6. *AS*; 7. *Stipa purpurea* [62]; 8. *Lygeum spartum* [47]; 9. *Kobresia pygmaea* [62]; 10. *Helictotrichon filifolium* [46]. The hollow circles represent cited results, and the solid ones refer to the results in this study.

Because not all of the tensile strength of the roots is mobilized instantaneously at the moment of bank failure [9,50,51,63], the product of RAR and T_r overestimates the true tensile strength (Table 3). As more and more fiber materials have been used in engineering practices, their ability to improve the tensile strength of the composite has been tested for natural fibers [24,64–67] and synthetic fibers [18,24,58,68]. It is generally believed that fiber materials can reinforce tensile strength, and the degree of reinforcement varies for different fiber materials. Tang et al. [3] proposed that the tensile strength of soil-fiber composite ($\sigma_{composite}$) includes two parts, which are the tensile strength of natural soils (σ_{soil}) and the increase of the tensile strength due to the fiber ($\Delta\sigma_{fiber}$):

$$\sigma_{composite} = \sigma_{soil} + \Delta\sigma_{fiber} \quad (4)$$

According to Zhu et al. [69], the tensile strength of unsaturated clays is 0.7~0.8 times that of the shear strength. In the current study, the ratio of tensile strength to the shear strength of soil without root is taken as 0.75, and the shear strength is 9.29 kPa [70]. Using these values and Equation (4), the reinforced tensile strengths of plant roots in AS and AM may be calculated as 60.43 and 15.0 kPa, respectively. The reinforcement of the healthy plant root system of AS is about 4 times higher than that of the AM. Also, they are less than the products of RAR and T_r by 11.58 and 4.36 kPa, respectively.

The relationship between the value of $\Delta\sigma_{fiber}$ for short (0.03 m) and long (0.05 m) fibers and different fiber contents [24] (Figure 10) was established by setting the root content of AS and AM as 0.48% and 0.18%, respectively [70]. It demonstrated a positive correlation between $\Delta\sigma_{fiber}$ and the fiber content [1,20,21,67], and showed that the longer the fiber length, the greater the strengthening effect [3,24]. In Figure 10, the points representing AS and AM are in line with the established relationship for the fiber lengths of 0.05 and 0.03 m, respectively. This consistency indicates that both the root length and root content contribute to $\Delta\sigma_{fiber}$, and both variables are higher for plants of AS than those for plants of AM.

Furthermore, the tensile strength may also be affected by the initial water content and dry bulk density. In the fiber-reinforced soils, it is negatively related to water content and positively related to dry bulk density [3,24]. The average density of the natural soil-root mixture for AS is 18% higher than that of AM (Table 2). This may be attributed to the decreased root number and the dramatically increased pore volume of surface soil (i.e, soil in the 0–0.05 m layer) [58]. Higher bulk density should increase not only bonding forces between particles, which enhances the tensile strength, but also the interfacial contact area of the fiber-matrix structure, which improves the interfacial shear strength and associated friction [24]. In theory, the bonding forces between particles and friction of the soil-root

mixture for AS is stronger than that of AM. Because the difference in the moisture content of the upper layer of soils between AS and AM is merely 1.43% (Table 2), its influence on the tensile strength of the soil-root mixture is relatively small. In this study, the influence of plant degradation on the soil tensile strength is mainly analyzed from a mechanical point of view, and the influences of soil properties (e.g., bulk density, moisture content, porosity, and particle size) on tensile strength and the impacts of degradation on hydraulic properties need to be further studied. It has been well known that the root system can change the hydraulic characteristics of soil [71–74], because it occupies the pore spaces of soil, thus reducing the porosity and increasing the water-holding capacity of soil [75]. In this study, the root number of AM decreased by about 46% compared with that of AS in the depth of 0–30 cm on the upper part of the riverbank, suggesting that the proportion of pores in the soil mass occupied by roots was reduced, which is evidenced by the fact that the density of soil mass was relatively lower than that of AS. Therefore, the water holding capacity of soil mass should be lower in AM than that in AS, implying that its suction of soil mass should also be lower [76].

According to Equation (4), the contributions of the root systems of AS and AM to the tensile strength of the soil-root mixture are 89.67% and 68.3%, respectively. This means that the influence of degradation on the tensile strength of the riverbank is mainly derived from the roots. In our study, when the AS degenerated to the AM, the rooted soil tensile strength decreased by 67.42% (Table 3). Li et al. [58] showed that the shear strength of the root-soil mixture decreases by 36.0% and 52.3% from severely degraded alpine meadows to moderately and slightly degraded alpine meadows, respectively. Thus, degradation of alpine swamp meadows obviously reduces the mechanical properties of the soils and weakens their ability to resist bank failure, wind and water erosion, and other external forces.

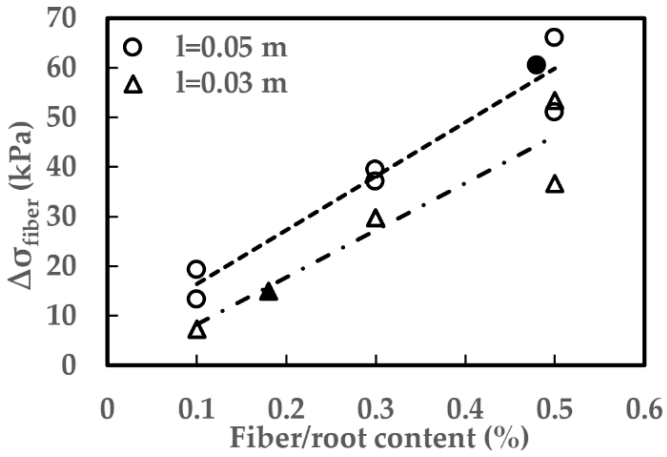

Figure 10. The relationship between fiber (root) content and reinforced tensile strength. The letter l in the diagram stands for the fiber length. The hollow circles and triangles are the data from Meriem et al. [24], while the solid circle and triangle refer to the reinforced tensile strength of AS and AM in this study, respectively.

4.2. The Role of Root System in Preventing Development of Riverbank Cracks

The development of cracks greatly destroys the integrity of the soil structure, weakens the mechanical properties of soils, reduces stability, increases permeability, intensifies evaporation, and increases soil erosion, resulting in a series of subsequent adverse effects on geotechnical engineering and the environment [77–80]. The tensile strength of the soil is an important mechanical parameter that controls the initiation and propagation of tensile cracks [3]. Therefore, enhancing the tensile strength of the soil and preventing the occurrence or slowing the expansion of cracks are critical for riverbank protection. Because plants in the AS have dense roots and strong single-root pullout resistance, they may enhance the tensile ductility of the rooted soils and inhibit the initial formation of tensile cracks. In our study, the expansion rate of tension cracks in cantilever arms due to weights

of the AS blocks and the duration of block failure are generally slower than those for the AM blocks. This indicates that types of riparian vegetation, fiber root number within the soils, and the root tensile strength may considerably constrain the number of cracks and their propagation rates [81].

When a tested block of cantilever arms is about to fail, a penetrating crack forms from the surface of AS or AM by following the path of least resistance (Figure 11). For the tested block of AS, the crack had a zigzag shape, and its length was about 1.24 m, which is longer than the crack length of AM by 0.14 m. The crack propagated with a preference angle until it was interrupted by roots. This angle seemed greater in the block with a higher root content. This property is consistent with the result of Meriem et al. [24]. At the depth of 0–0.3 m, the root number of AS that passing through the collapsed profile was 1.84 times that of the root number of AM (Figure 6). As a result, a crack in AS propagated in a way that avoided most roots. Given that the length of the crack was longer than that of AM, the time needed to penetrate through the soil-root mixture is longer. Nonetheless, the crack pattern is smoother on the surface of the AM block because of its lower number of roots.

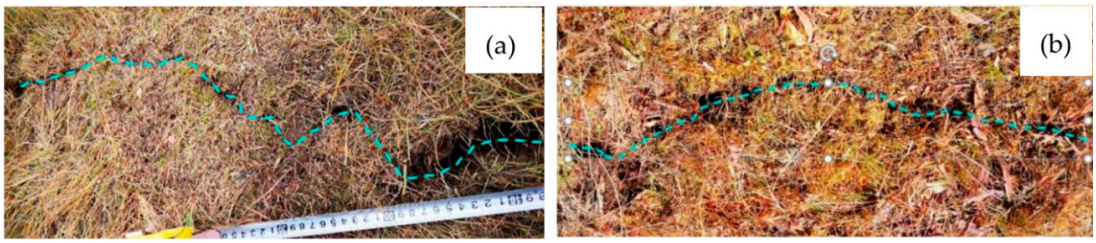

Figure 11. The planform crack pattern at the surface of the block in (**a**) AS and (**b**) AM.

Considering the impact of the degraded alpine swamp meadow on tensile strength of riverbank in the UYR region, the grassland management should practice regional rotation grazing, rational distribution of herds, and balanced use of the riparian alpine swamp meadow. In addition, anthropogenic disturbances, in particular engineering construction, should be reduced as much as possible.

5. Conclusions

Under the influence of climate change and increased anthropogenic disturbances, the alpine swamp meadow (AS), which is the main type of vegetation cover in the meandering riverbank of the Upper Yellow River (UYR), is subject to severe degradation and typically has transformed into the alpine meadow (AM). However, little is known about the tensile strength of the roots in soils and the influence of riparian vegetation degradation on the tensile strength of riverbanks. To reflect the actual interaction between soils and the roots with the natural root branching structure for AS and AM and its effect on bank strength, we measured properties of root vertical distribution and number and performed in situ root pullout and artificial excavation tests. Our results led to the following conclusions. First, though spatial and size distributions of roots in the soil-root mixture of AS and AM were similar, AS was characterized by a higher number of roots than AM. Second, the tensile strength of individual roots decreased with the diameter of roots in both AS and AM. Yet, the former always had higher tensile strength than the latter for any given root diameter. Similarly, the tensile strength of the soil-root mixture in AS was about three times higher than that in AM. This difference is mainly caused by the fact that the lateral extended and wave-shaped root structure in AS is more effective in enhancing the resistance of the soil-root mixture to the external force than the simple vertically distributed root structure in AM. Third, the tensile crack developed in the collapsed block for AM was deeper than that for AS, indicating the reduced resistance to the external force as AS gradually degraded to AM. The impact of the roots for the degraded vegetation (i.e., AM) was also reflected by the relatively smooth and shorter crack route on the surface of the collapsed block for AM. These findings call for better ecological management for preventing AS from being degraded to AM.

Although grassland degradation is a worldwide problem [82,83], how such degradation affects the mechanical properties of riparian riverbanks in the alpine environment has not been fully understood.

Our study provides firsthand evidence of weakened bank strength in the soil-root mixture due to degradation of vegetation and will serve as a benchmark for future investigation of riverbank strength, not only in the UYR, but also in other alpine regions in the world.

Author Contributions: Conceptualization, H.Z. and P.G.; Data curation, H.Z., G.L.; Formal analysis, H.Z., P.G.; Funding acquisition, H.Z., Z.L., G.L. and X.L.; Investigation, H.Z., Z.L., J.F., G.L., Y.L. and X.H.; Methodology, H.Z., P.G. and Z.L.; Project administration, H.Z.; Resources, X.L., G.L. and J.F.; Writing—original draft, H.Z.; Writing—review & editing, P.G. All authors have read and agreed to the published version of the manuscript.

Funding: This research was funded by the National Natural Science Foundation of China (Grant No. 41302258, 41762023, 41662023, and 51979012), the Project of Qinghai Science & Technology Department (Grant No. 2017-ZJ-776), the Natural Science Foundation Innovation Team Project of Qinghai Provincial Department of Science and Technology (Grant No. 2020-ZJ-904).

Acknowledgments: The authors thank undergraduate students B.L., B.X., R.Z. and Y.G. for data collection in the field. Thanks are extended to the anonymous reviewers and Editor for useful comments that improved the manuscript.

Conflicts of Interest: The authors declare no conflict of interest.

References

1. Ziegler, S.; Leshchinsky, D.; Ling, H.L.; Perry, E.B. Effect of short polymeric fibers on crack development in clays. *Soils Found.* **1998**, *38*, 247–253. [CrossRef]
2. Li, G.X.; Chen, L. Study of centrifugal model tests on texsol and cohesive soil slopes. *Chin. J. Geotech. Eng.* **1998**, *20*, 12–15. (In Chinese)
3. Tang, C.S.; Wang, D.Y.; Cui, Y.Y. Tensile Strength of Fiber reinforced soil. *Mater. Civ. Eng.* **2016**, *28*, 1–13. [CrossRef]
4. Divya, P.V.; Viswanadham, B.V.S.; Gourc, J.P. Evaluation of tensile strength-strain characteristics of fiber reinforced soil through laboratory tests. *J. Mater. Civ. Eng.* **2014**, *26*, 14–23. [CrossRef]
5. Simon, A.; Curini, A.; Darby, S.E.; Langendoen, E.J. Bank and near-bank processes in an incised channel. *Geomorphology* **2000**, *35*, 193–217. [CrossRef]
6. Schmidt, K.M.; Roering, J.J.; Stock, J.D.; Dietrich, W.E.; Montgomery, D.R.; Schaub, T. The variability of root cohesion as an influence on shallow landslide susceptibility in the Oregon Coast Range. *Can. Geotech. J.* **2001**, *38*, 995–1024. [CrossRef]
7. Roering, J.J.; Schmidt, K.M.; Stock, J.D.; Dietrich, W.E.; Montgomery, D.R. Shallow landsliding, root reinforcement, and the spatial distribution of trees in the Oregon Coast Range. *Can. Geotech. J.* **2003**, *40*, 237–253. [CrossRef]
8. Hubble, T.C.T.; Docker, B.B.; Rutherford, I.D. The role of riparian trees in maintaining riverbank stability: A review of Australian experience and practice. *Ecol. Eng.* **2010**, *36*, 292–304. [CrossRef]
9. Abernethy, B.; Rutherford, I.D. Where along a river's length will vegetation most effectivelystabilise stream banks? *Geomorphology* **1998**, *23*, 55–75. [CrossRef]
10. Thorne, C.R.; Tovey, N.K. Stability of composite river banks. *Earth Surf. Process. Landf.* **1981**, *6*, 469–484. [CrossRef]
11. Abernethy, B.; Rutherford, I.D. The distribution and strength of riparian tree roots in relation to riverbank reinforcement. *Hydrol. Process.* **2001**, *15*, 63–79. [CrossRef]
12. Simon, A.; Collison, A.J.C. Quantifying the mechanical and hydrologic effects of riparian vegetation on streambank stability. *Earth Surf. Process. Landf.* **2002**, *27*, 527–546. [CrossRef]
13. Yu, G.A.; Li, Z.; Yang, H.; Lu, J.; Huang, H.Q.; Yi, Y. Effects of riparian plant roots on the unconsolidated bank stability of meandering channels in the Tarim River, China. *Geomorphology* **2020**, *351*, 106958. [CrossRef]
14. Van De Wiel, M.J.; Darby, S.E. A new model to analyse the impact of woody riparian vegetation on the geotechnical stability of riverbanks. *Earth Surf. Proc. Landf.* **2007**, *32*, 2185–2198. [CrossRef]
15. Parker, G.; Shimizu, Y.; Wilkerson, G.V.; Eke, E.C.; Abad, J.D.; Lauer, J.W.; Paola, C.; Dietrich, W.E.; Voller, V.R. A new framework for modeling the migration of meandering rivers. *Earth Surf. Proc. Landf.* **2011**, *36*, 70–86. [CrossRef]
16. Zhu, H.L.; Hu, X.S.; Li, Z.W.; Song, L.; Li, K.; Li, X.L.; Li, G.R. The influences of riparian vegetation on bank failures of a small meadow-type meandering river. *Water* **2018**, *10*, 692. [CrossRef]

17. Abernethy, B.; Rutherford, I.D. The effect of riparian tree roots on the mass-stability of riverbanks. *Earth Surf. Process. Landf.* **2000**, *25*, 921–937. [CrossRef]
18. Samadi, A.; Amiri-Tokaldany, E.; Davoudi, M.H.; Darby, S.E. Experimental and numerical investigation of the stability of overhanging riverbanks. *Geomorphology* **2013**, *184*, 1–19. [CrossRef]
19. Lawton, E.C.; Khire, M.V.; Fox, N.S. Reinforcement of Soils by Multi-oriented Geo-synthetic Inclusions. *J. Geotech. Eng.* **1993**, *119*, 257–275. [CrossRef]
20. Plé, O.; Lê, T.N.H. Effect of polypropylene fiber reinforcement on the mechanical behavior of silty clay. *Geotext. Geomembr.* **2012**, *32*, 111–116. [CrossRef]
21. Mesbah, A.; Morel, J.C.; Walker, P.; Ghavami, K. Development of a direct tensile test for compacted earthblocks reinforced with natural fibers. *J. Mater. Civ. Eng.* **2004**, *16*, 95–98. [CrossRef]
22. Onur Akaya, A.; Özera, T.; Foxb, G.A.; Wilson, G.V. Application of fibrous streambank protection against groundwater seepage erosion. *J. Hydrol.* **2018**, *565*, 27–38. [CrossRef]
23. Das, N.; Singh, S.K. Geotechnical behaviour of lateritic soil reinforced with brown waste and synthetic fiber. *Int. J. Geotech. Eng.* **2019**, *13*, 287–297. [CrossRef]
24. Meriem, C.; Houda, G.; Mehrez, J. Tensile behaviour analysis of compacted clayey soil reinforced with natural and synthetic fibers: Effect of initial compaction conditions. *Eur. J. Environ. Civ. Eng.* **2020**, *24*, 354–380.
25. Wu, T.H.; McKinnell, W.P., III; Swanston, D.N. Strength of tree roots and landslides on Prince of Wales Island, Alaska. *Can. Geotech. J.* **1979**, *16*, 19–33. [CrossRef]
26. Waldron, L.J.; Dakessian, S. Soil reinforcement by roots: Calculation of increased soil shear resistance from root properties. *Soil Sci.* **1981**, *132*, 427–435. [CrossRef]
27. Pollen, N.; Simon, A. Estimating the mechanical effects of riparian vegetation on stream bank stability using a fiber bundle model. *Water Resour. Res.* **2005**, *41*, 1–11. [CrossRef]
28. Schwarz, M.; Lehmann, P.; Or, D. Quantifying lateral root reinforcement in steep slopes: From a bundle of roots to tree stands. *Earth Surf. Proc. Landf.* **2010**, *35*, 354–367. [CrossRef]
29. Li, Y.Z.; Fu, J.T.; Yu, D.M.; Hu, X.S.; Zhu, H.L.; Li, G.Y.; Hu, X.T. Mechanical effects of halophytes roots and optimal root content for slope protection in cold and arid environment. *Chin. J. Rock Mech. Eng.* **2015**, *34*, 1370–1383. (In Chinese)
30. Liu, Y.B.; Hu, X.S.; Yu, D.M.; Li, S.X.; Yang, Y.Q. Microstructural features and friction characteristics of the interface of shrub roots and soil in loess area of Xining Basin. *Chin. J. Rock Mech. Eng.* **2018**, *37*, 1270–1280. (In Chinese)
31. Li, Z.W.; Yu, G.A.; Xu, M.Z.; Hu, X.Y.; Yang, H.M.; Hu, S.X. Progress in studies on river morphodynamics in Qinghai-Tibet Plateau. *Adv. Water Sci.* **2016**, *27*, 617–628.
32. Li, J.; Zhang, F.W.; Lin, L.; Li, H.Q.; Du, Y.G.; Li, Y.K.; Cao, G.M. Response of the plant community and soil water status to alpine *Kobresia* meadow degradation gradients on the Qinghai–Tibetan Plateau, China. *Ecol. Res.* **2015**, *30*, 589–596. [CrossRef]
33. Wang, G.X.; Wang, Y.B.; Li, Y.S.; Cheng, H.Y. Influences of alpine ecosystem responses to climatic change on soil properties on the Qinghai-Tibet Plateau, China. *Catena* **2007**, *70*, 506–514. [CrossRef]
34. Wang, G.X.; Liu, G.S.; Li, C.J. Effects of changes in alpine grassland vegetation cover on hillslope hydrological processes in a permafrost watershed. *J. Hydrol.* **2012**, *444–445*, 22–33.
35. Zeng, C.; Zhang, F.; Wang, Q.J.; Chen, Y.Y.; Joswiak, D.R. Impact of alpine meadow degradation on soil hydraulic properties over the Qinghai-Tibetan Plateau. *J. Hydrol.* **2013**, *478*, 148–156. [CrossRef]
36. Pan, T.; Hou, S.; Wu, S.H.; Liu, Y.J.; Liu, Y.H.; Zou, X.T.; Herzberger, A.; Liu, J.G. Variation of soil hydraulic properties with alpine grassland degradation in the eastern Tibetan Plateau. *Hydrol. Earth Syst. Sci.* **2017**, *21*, 2249–2261. [CrossRef]
37. Krzeminska, D.; Kerkhof, T.; Skaalsveen, K.; Stolte, J. Effect of riparian vegetation on stream bank stability in small agricultural catchments. *Catena* **2019**, *172*, 87–96. [CrossRef]
38. Duan, S.Q. Runoff spatial difference of small-scale in Huangnan, Qinghai province and its cause. *Adv. Water Sci.* **2016**, *27*, 11–21.
39. Yu, Z.X. Investigation of variety resources of Oula sheep at Henan county in Qinghai province. *Anim. Husb. Feed Sci.* **2009**, *30*, 120–124. (In Chinese)
40. Ren, G.H.; Deng, B.; Hou, Y. Changes of community characteristics in the degradation process of the alpine swamp wetland in the Yellow River Source area. *Pratacult. Sci.* **2015**, *32*, 1222–1229. (In Chinese)

41. Xie, B.S.; Zhu, H.L.; Li, B.F.; Hu, X.S. Study on relationship between vegetation spatial distribution and soil properties in the meander riverside in source region of the Yellow River. *J. Sediment Res.* **2019**, *44*, 66–73. (In Chinese)
42. Schenk, H.J.; Jackson, R.B. Rooting depths, lateral root spreads and below-ground/above-ground allometries of plants in water-limited ecosystems. *J. Ecol.* **2002**, *90*, 480–494. [CrossRef]
43. Ministry of Construction. *GB/T 50123–1999. Standard for Soil Test Method*; Ministry of Construction: Beijing, China, 2010.
44. Xia, J.Q.; Zong, Q.L.; Xu, Q.X.; Deng, C.Y. Soil properties and erosion mechanisms of composite riverbanks in Lower Jingjiang Reach. *Adv. Water Sci.* **2013**, *24*, 810–820. (In Chinese)
45. Ajaz, A. Stress-Strain Behaviour of Compacted Clays in Tension and Compression. Ph.D. Thesis, Cambridge University, Cambridge, MA, USA, 1973.
46. Baets, S.D.; Poesen, J.; Reubens, B.; Wemans, K.; Baerdemaeker, J.D.; Muys, B. Root tensile strength and root distribution of typical Mediterranean plant species and their contribution to soil shear strength. *Plant Soil* **2008**, *305*, 207–226. [CrossRef]
47. Mattia, C.; Bischetti, G.B.; Gentile, F. Biotechnical characteristics of root systems of typical Mediterranean species. *Plant Soil* **2005**, *278*, 23–32. [CrossRef]
48. Bischetti, G.B.; Chiaradia, E.A.; Simonato, T.; Speziali, B.; Vitali, B.; Vullo, P.; Zocco, A. Root strength and root area ratio of forest species in Lombardy (Northern Italy). *Plant Soil* **2005**, *278*, 11–22. [CrossRef]
49. Docker, B.B.; Hubble, T.C.T. Quantifying root-reinforcement of river bank soils by four Australian tree species. *Geomorphology* **2008**, *100*, 401–418. [CrossRef]
50. Lawrence, C.J.; Rickson, R.J.; Clark, J.E. The effect of grass roots on the shear strength of colluvial soils in Nepal. In *Advances in Hillslope Processes*; Anderson, M.G., Brooks, S.M., Eds.; John Wiley and Sons: Chichester, UK, 1996; Volume 2, pp. 857–868.
51. Reubens, B.; Poesen, J.; Danjon, F.; Geudens, G.; Muys, B. The role of fine and coarse roots in shallow slope stability and soil erosion control with a focus on root system architecture: A review. *Trees* **2007**, *21*, 385–402. [CrossRef]
52. Schwarz, M.; Cohen, D.; Or, D. Soil-root mechanical interactions during pullout and failure of root bundles. *Geophys. Res.* **2010**, *115*, 1–19. [CrossRef]
53. Schwarz, M.; Preti, F.; Giadrossich, F.; Lehmann, P.; Or, D. Quantifying the role of vegetation in slope stability: A case study in Tuscany (Italy). *Ecol. Eng.* **2010**, *36*, 285–291. [CrossRef]
54. Zhu, J.Q.; Wang, Y.Q.; Wang, Y.J.; Zhang, H.L.; Li, Y.P.; Li, Y. An analysis on soil physical enhancement effects of root system of *PinusTabulaeformis* and *Acer Truncatum* based on two models. *Bull. Soil Water Conserv.* **2015**, *35*, 277–282. (In Chinese)
55. Li, X.L.; Perry, G.L.W.; Brierley, G.; Sun, H.Q.; Li, C.H.; Lu, G.X. Quantitative assessment of degradation classifications for degraded alpine meadows (heitutan), Sanjiangyuan, Western China. *Land Degrad. Dev.* **2014**, *25*, 417–427. [CrossRef]
56. Cheng, H.Y.; Wang, G.X.; Hu, H.C.; Wang, Y.B. The variation of soil temperature and water content of seasonal frozen soil with different vegetation coverage in the headwater region of the Yellow River, China. *Environ. Geol.* **2008**, *54*, 1755–1762. [CrossRef]
57. Niu, Y.J.; Zhou, J.W.; Yang, S.W.; Chu, B.; Zhu, H.M.; Zhang, B.; Fang, Q.G.; Tang, Z.S.; Hua, L.M. Plant diversity is closely related to the density of zokor mounds in three alpine rangelands on the Tibetan Plateau. *PeerJ* **2019**, *7*, e6921. [CrossRef]
58. Li, G.R.; Li, X.L.; Chen, W.T.; Li, J.F.; Zhu, H.L.; Hu, X.S.; Zhou, H.K.; Sun, H.Q. Effects of degradation severity on the physical, chemical and mechanical properties of topsoil in alpine meadow on the Qinghai-Tibet Plateau, west China. *Catena* **2020**, *187*, 104370. [CrossRef]
59. Tang, C.S.; Li, J.; Wang, D.Y.; Shi, B. Investigation on the interfacial mechanical behavior of wave-shaped fiber reinforced soil by pullout test. *Geotext. Geomembr.* **2016**, *44*, 872–883. [CrossRef]
60. Li, Y.; Zhu, X.M.; Tian, J.Y. The effectiveness of plant roots in improving soil anti-scourability on the loess plateau. *Sci. Bull.* **1991**, *12*, 935–938. (In Chinese)
61. Zhou, Y.; Watts, D.; Cheng, X.P.; Li, Y.H.; Luo, H.S.; Xiu, Q. The traction effect of lateral roots of Pinus yunnanensis on soil reinforcement: A direct in situ test. *Plant Soil* **1997**, *190*, 77–86. [CrossRef]

62. Li, G.Y.; Hu, X.T.; Li, X.L.; Yu, D.M.; Fu, J.T.; Zhu, H.L.; Hu, X.S. Mechanical Effects of Alpine Grassland Plants in Slope Protection in Maqin County of the Source Area of the Yellow River. *Mt. Res. Dev.* **2014**, *32*, 550–560. (In Chinese)
63. Comino, E.; Druetta, A. The effect of Poaceae roots on the shear strength of soils in the Italian alpine environment. *Soil Tillage Res.* **2010**, *106*, 194–201. [CrossRef]
64. Bessadok, A.; Roudesli, S.; Marais, S.; Follain, N.; Lebrun, L. Alfa fibers for unsaturated polyester composites reinforcement: Effects of chemical treatments on mechanical and permeation properties. *Compos. Part A* **2009**, *40*, 184–195. [CrossRef]
65. Tran, H.N.; Shinji, O.; Nguyen, H.T.; Satoshi, K. Effect of alkali treatment on interfacial and mechanical properties of coir fiber reinforced poly(butylene succinate) biodegradable composites. *Compos. Part B* **2011**, *42*, 1648–1656.
66. Parisi, F.; Asprone, D.; Fenu, L.; Prota, A. Experimental characterization of Italian composite adobe bricks reinforced with straw fibers. *Compos. Struct.* **2015**, *122*, 300–307. [CrossRef]
67. Khiem, Q.T.; Tomoaki, S.; Hiroshi, T. Improvement of mechanical behavior of cemented soil reinforced with waste cornsilk fibers. *Constr. Build. Mater.* **2018**, *178*, 204–210.
68. Tang, C.S.; Shi, B.; Cai, Y.; Gao, W.; Chen, F.J. Experimental study on polypropylene fiber improving soft soils. *Rock Soil Mech.* **2007**, *28*, 1796–1800. (In Chinese)
69. Zhu, C.H.; Liu, J.M.; Yan, B.W.; Ju, J.L. Experimental study on relationship between tensile and shear strength of unsaturation clay earth material. *Chin. J. Rock Mech. Eng.* **2008**, *27* (Suppl. S2), 3453–3458. (In Chinese)
70. Li, B.F.; Zhu, H.L.; Xie, B.S.; Luo, L.Y.; Li, G.R.; Hu, X.S. Study on tensile properties of root-soil composite of alpine meadow plants in the riparian zone of the Yellow River source region. *Chin. J. Rock Mech. Eng.* **2020**, *39*, 424–432. (In Chinese)
71. Leung, A.K.; Garg, A.; Ng, C.W.W. Effects of plant roots on soil–water retention and induced suction in vegetated soil. *Eng. Geol.* **2015**, *193*, 183–197. [CrossRef]
72. Ng, C.W.W.; Leung, A.K.; Woon, K.X. Effects of soil density on grass-induced suction distributions in compacted soil subjected to rainfall. *Can. Geotech. J.* **2014**, *51*, 311–321. [CrossRef]
73. Gabrm, A.; Akran, M.; Taylor, H.M. Effect of simulated roots on the permeability of silty soil. *Geotech. Test. J.* **1995**, *18*, 112–115.
74. Huat, B.B.K.; Alif, H.J.; Low, T.H. Water infiltration characteristics of unsaturated soil slope and its effect on suction and stability. *Geotech. Geol. Eng.* **2006**, *24*, 1293–1306. [CrossRef]
75. Ng, C.W.W. Atmosphere-plant-soil interactions: Theories and mechanisms. *Chin. J. Geotech. Eng.* **2017**, *39*, 1–47. (In Chinese)
76. Pollen, N.; Simon, A. Hydrologic and hydraulic effects of riparian root networks on streambank stability: Is mechanical root-reinforcement the whole story? *Geomorphology* **2010**, *116*, 353–362. [CrossRef]
77. Morris, P.H.; Graham, J.; Wiliams, D.J. Cracking in drying soils. *Can. Geotech. J.* **1992**, *29*, 263–277. [CrossRef]
78. Albrecht, B.A.; Benson, C.H. Effect of desiccation on compacted natural clays. *J. Geotech. Geoenviron.* **2001**, *127*, 67–75. [CrossRef]
79. Peron, H.; Hueckel, T.; Laloui, L.; Hu, L.B. Fundamentals of desiccation cracking of fine-grained soils: Experimental characterization and mechanisms identification. *Can. Geotech. J.* **2009**, *46*, 1177–1201. [CrossRef]
80. Tang, C.S.; Shi, B.; Liu, C.; Zhao, L.Z.; Wan, B.J. Influencing factors of geometrical structure of surface shrinkage cracks in clayey soils. *Eng. Geol.* **2008**, *101*, 204–217. [CrossRef]
81. Miller, C.J.; Rifai, S. Fiber reinforcement for waste containment soil liners. *J. Environ. Eng.* **2004**, *130*, 891–895. [CrossRef]
82. Muller, S.; Dutoit, T.; Alard, D.; Grévilliot, F. Restoration and rehabilitation of species-rich grassland ecosystems in France: A review. *Restor. Ecol.* **1998**, *6*, 94–101. [CrossRef]
83. Carrick, P.J.; Krüger, R. Restoring degraded landscapes in lowland Namaqualand: Lessons from the mining experience and from regional ecological dynamics. *J. Arid Environ.* **2007**, *70*, 767–781. [CrossRef]